SECTION 2: ESTIMATION OF MAGNETISATION DIRECTION FROM MAGNETIC FIELD ANALYSIS AND INVERSION

This page intentionally left blank

5
Expression of remanent magnetisation in magnetic field data: recognition, analysis and inversion

C.A. Foss

ABSTRACT

The first question to address in analysis or inversion of magnetic field data is whether that magnetisation is oriented parallel to the geomagnetic field or in a different direction. For a well-isolated magnetisation it may be possible to make this determination from the pattern of its magnetic field variation but in more complicated cases the field of the magnetisation must first be separated from overlapping fields of adjacent magnetisations. This is an interpretive process and if the separation is incorrect then the resulting magnetisation direction estimates will also be incorrect. Challenges in separation of magnetic fields increase with complexity in the distribution of magnetisation and with complexity of the fields with which they overlap. However, for correctly separated magnetic fields there is considerable tolerance in estimation of the mean magnetisation direction, and reliable estimates of magnetisation direction should be obtained from the wide range of available analysis and inversion methodologies. Expectation should only be to recover a single representative magnetisation direction for each discrete, compact feature in the magnetic field.

5.1 IS ESTIMATION OF MAGNETISATION DIRECTION FROM MAGNETIC FIELD DATA JUSTIFIED?

Until the start of the new millennium there was widespread scepticism that magnetisation direction could be reliably recovered from magnetic field data. This doubt was the legacy from times when magnetic field analysis was largely confined to profile data using master curves computed for highly elongated 'two-dimensional' magnetisations. For thin planar sheets of magnetisation the dip of the sheet combines with the inclination of magnetisation into a single angular term from which neither can be resolved without knowledge of the other (Hood 1964). It has long been known that reverse polarity magnetisations generate magnetic field anomalies of opposite sign to those expected from normal polarity magnetisation, but these anomalies were considered mostly in terms of their polarity (as an apparent negative magnetic susceptibility) rather than more generally in terms of direction of magnetisation. Relationships between magnetisation direction and the pattern of magnetic field variation were reported in a three-dimensional modelling study by Zietz and Andreasen (1967). In the steep northern geomagnetic fields they studied, they noted that declination of magnetisation is revealed by the azimuth of the line from the anomaly peak to trough and inclination is revealed by the peak and trough amplitude ratio.

The only analytic proof that magnetisation direction can be recovered from magnetic field data was developed by Helbig (1963). The two conditions of Helbig's analytic proof are that the magnetisation is a dipole and that its horizontal location is known. An analysis of magnetisation direction based on this proof is illustrated in Fig. 5.1. The three orthogonal magnetic field components can be

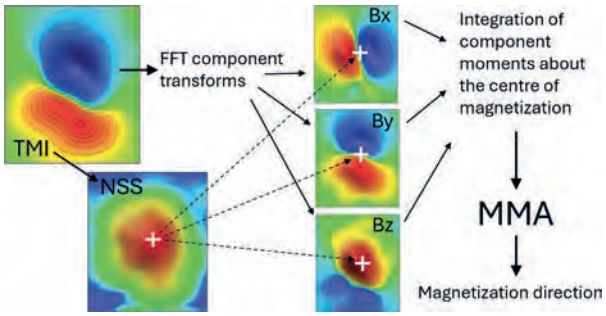

Fig. 5.1. Schematic of Helbig magnetic moment analysis (MMA) using integrals of components obtained by FFT phase transform of TMI data about the centre of magnetisation derived from the NSS transform.

mapped by appropriate phase transforms of the TMI grid (Lourenço and Morrison 1973; Blakely 1995). The moments of these components are then determined by numerical integration about a supplied horizontal centre of magnetisation, and those integrals are substituted into Helbig's equations. Estimation of magnetisation is over-prescribed from the three integrals, providing consistency measures. The integrals should be taken to infinity but experimentation shows that magnetisation direction can be correctly estimated from small field samples provided they are correctly centred. Schmidt and Clark (1998) and Clark (2014) provide correction factors for the magnitude of the magnetic moment as a function of the ratio of grid side length to depth to the centre of magnetisation. Helbig's analysis was not widely applied until Schmidt and Clark (1997) proposed the computerised form of the analysis illustrated in Fig. 5.1. Foss and McKenzie (2011) investigated Helbig analysis in a study of the Black Hill Norite anomaly and were able to recover magnetisation directions similar to those determined from inversion of the same magnetic field data and consistent with nearby direct palaeomagnetic measurements (Rajagopalan *et al*. 1993; Schmidt *et al*. 1993). Using the same magnetic field data Phillips (2005) published an automated version of Helbig analysis that attempted to isolate magnetisation directions by searching for stable directions in analysis of arrays of overlapping windows of different sizes. However, because of the high sensitivity to the centre of the analysis, this search method was only partially successful.

The two-dimensional total gradient transform (also known as the two-dimensional analytic signal) peaks over a compact magnetisation irrespective of its magnetisation direction (Nabighian 1972). The three-dimensional total gradient is not perfectly independent of magnetisation direction but has low sensitivity to it, particularly for compact magnetic field anomalies. The normalised source strength (NSS) (Beiki *et al*. 2012) has proven independence to magnetisation direction for a dipole anomaly. Therefore, if an NSS transform is applied to a TMI grid of a dipole magnetisation to locate its centre, Helbig analysis can be performed using that estimated centre.

Since the turn of the millennium there has been a sharp increase in the number of determinations of magnetisation using parametric or voxel inversions. This marks an abrupt change to widespread confidence that magnetisation direction can be automatically recovered from any sample of magnetic field data. I propose that meaningful magnetisation direction estimates can only be made from suitable magnetic field measurements above suitable concentrations of magnetisation (magnetisation direction 'sweet-spots'). Empirical tests have established that modest departure of the distribution of magnetisation from a dipole (the proven case for Helbig analysis) causes only modest reduction in resolution of magnetisation direction. If, for instance, the spherical source of a dipole is relaced by an ellipsoid, the reliability in estimating magnetisation direction by Helbig analysis decreases gradually with increasing difference in ratio of the axes (particularly the horizontal axes). Extremely large axial ratios, as noted for thin sheets, are least suitable for estimation of magnetisation direction from magnetic field data. Location of the centre of magnetisation from total gradient or NSS transform of magnetic field data similarly loses resolution gradually as the distribution of magnetisation progressively departs from that of a dipole.

Figure 5.2 is a schematic representation of the population of magnetic anomalies in an area as a function of

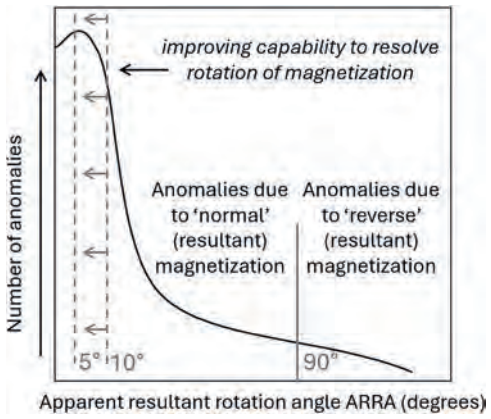

Fig. 5.2. Schematic of the population of anomalies within an area with magnetisation directions rotated away from the geomagnetic field.

difference in their magnetisation direction from the local geomagnetic field (the apparent resultant rotation angle, 'ARRA'). The shape of a curve varies with the geological ages of the magnetisations in an area, with the spatial distributions of those magnetisations and with the resolution with which the magnetic field is mapped. Many anomalies are due to magnetisations dominated by induced and/or 'soft' viscous remanent magnetisation of the same direction and have resultant magnetisation directions close to the geomagnetic field direction. For angular separations up to at least 90° the number of anomalies falls with increasing separation from the geomagnetic field. In areas of recent volcanic or subvolcanic rocks there may be a secondary peak in the population marking reverse remanent magnetisation. As indicated in Fig. 5.2, the significance of apparent deviation of a magnetisation direction from the geomagnetic field tests an increasing number of anomalies if analyses or inversions can be performed with high sensitivity. At present the resolution at which it is feasible to assign meaning to a magnetisation direction or compare magnetisation directions derived from magnetic field data is of the order of 5° in optimum cases but is more typically between 10° and 15°. An extensive review of the wide range of methods for determination of magnetisation direction is given by Clark (2014) and the highest resolution is achieved by dedicated user-guided inversion of isolated anomalies.

The widespread concept that magnetisation direction can be mapped continuously is a fallacy. Models with continuous variation in magnetisation direction may match the measured field well and may even closely represent the true magnetisation of the ground but they cannot be known to be valid. From stepwise demagnetisation of palaeomagnetic samples we know that the 1 inch diameter, 1 inch high cylinders can carry multiple over-printed remanent magnetisations of quite different direction that from their external magnetic field appear to be a single homogeneous magnetisation, and the same vector summation applies to closely adjacent magnetisations at much larger scales. However, without independent information there is no justification to propose multiple magnetisations to explain a magnetic field feature that can be acceptably explained by a single magnetisation. In the case that two magnetisations of different direction are present, local magnetisations due to their combination do not generate a cloud of directions, but directions smeared along the segment of a great circle between the two directions.

5.2 KEY POINTS RELATING MAGNETISATION DIRECTION AND MAGNETIC FIELDS

There are several key points in analysis of magnetisation direction from magnetic field data:

- Spatial variation in magnetic fields is due to spatial variation in either intensity or direction of magnetisation
- Many magnetisations causing prominent, discrete magnetic field variations are sufficiently strong that magnetic field analysis provides reasonable estimates of their absolute value rather than just their contrast with surrounding magnetisation
- The external magnetic field of a magnetisation is an expression of the vector sum of its induced and remanent magnetisations. In most cases, induced magnetisation is parallel to the local geomagnetic field but it can be deflected by anisotropy of magnetic susceptibility (AMS) or self-demagnetisation effects. The direction of remanent magnetisation depends on its acquisition age and any subsequent rotations by continental drift or tectonic forces
- Values of the Koenigsberger ratio of remanent to induced magnetisation are highly variable but many measurements of magnetic susceptibility and remanent magnetisation return values between 0.3 and 3.0. In magnetic field inversion it is unjustified to ignore remanent magnetisation because it is unknown or is perceived to be problematic
- As a scalar, the Koenigsberger ratio of the strength of remanent to induced magnetisation is insufficient to describe the vector relationships between remanent, induced and resultant magnetisations and this statistic should be supplemented with the Apparent Resultant Rotation Angle (ARRA) that is a measure of the rotation of the resultant magnetisation away from the local geomagnetic field direction
- ARRA is the statistic most critical in determining the ease of recognition of remanent magnetisation in magnetic field data. A large rotation angle requires a moderate to large Koenigsberger ratio, but a large Koenigsberger ratio does not necessarily produce a large rotation angle
- Coarse-grained, multi-domain magnetite generally carries a viscous remanent magnetisation in the present field direction. This remanent magnetisation cannot be discriminated from induced magnetisation in (static) magnetic field data and is undetected by magnetic susceptibility measurements. Inversions

imposing magnetisation based only on magnetic susceptibility measurements constrains those inversions to give incorrect answers even if the remanent magnetisation does not rotate the resultant magnetisation direction
- There are only selected locations in a magnetic field ('sweet-spots') where the magnetic field data support reliable detection of magnetisation direction. Each sweet-spot supports estimation of a single magnetisation direction (the mean direction of that magnetisation)
- In steep northern geomagnetic inclinations and for equidimensional anomalies the declination of resultant magnetisation is indicated by the anomaly peak-to-trough azimuth, and in steep southern geomagnetic inclinations it is indicated by the anomaly trough-to-peak azimuth
- In the same steep-inclination fields, a high peak-to-trough amplitude ratio indicates a steep-inclination magnetisation with the same polarity as the field and a high trough-to-peak amplitude ratio indicates a steep-inclination magnetisation with opposite polarity to the field. A peak-to-trough amplitude ratio close to parity indicates a low-inclination magnetisation
- These relationships support estimation of magnetisation direction from visual inspection of the magnetic field in high geomagnetic inclination fields. At low geomagnetic inclination it is also possible to predict magnetisation from the pattern of well-defined anomalies but the relationships are more complex
- If you cannot recognise the presence of remanent magnetisation from visual inspection of well-imaged magnetic field data (especially with the benefit of subdued or extinguished sun-shading and a contour overlay) you should not expect inversion to find it for you
- It is a fallacy that voxel inversion can recover magnetisation direction of each voxel in a model. The fields computed from those models may match the measured magnetic field but their apparent detail cannot be justified from magnetic field data alone
- The greatest challenge in estimation of magnetisation direction from magnetic field data is to effectively separate the field variation due to that magnetisation from other field variations. Field separations are invariably interpretive, even if analytical methods are applied to effect their separation
- A major trade-off against magnetisation direction in the inversion of magnetic field data is its horizontal position. If a magnetic field is inverted with an incorrect magnetisation direction the estimated horizontal location of the magnetisation will be incorrect, and conversely if horizontal location of the magnetisation is incorrect then inversion will give an incorrect magnetisation direction
- Incorrect estimation of the structural dip or plunge of a magnetisation also trades off against estimation of its magnetisation direction. This is because change of the dip or plunge of a magnetisation causes change in its horizontal position with depth. The problem is more extreme for a thin sheet of magnetisation than for a narrow pipe
- Vertical location and depth extent of magnetisation do not strongly trade-off against estimated direction. However, if error in estimated depth or depth extent gives rise to substantial misfit between measured and model-computed fields those misfits can accommodate error in estimating magnetisation direction even though they do not cause it
- The influence of shape of a distribution of magnetisation complicates estimation of its magnetisation direction. This problem is more acute in 'proximal' fields close to the magnetisation and eases with distance in 'distal' fields. In the ultimate distal field an anomaly (if still detectable and sufficiently defined for reliable analysis) is identical to that of a co-centred dipole magnetisation of identical magnetic moment
- If we can improve capability to determine source magnetisation direction from analysis or inversion of magnetic field data then correlation of magnetisation direction estimates will become a valuable method to map the regional extent of igneous, metamorphic, thermal and mineralising events
- The Australian remanent anomalies database is a resource to report magnetisation direction estimates recovered from magnetic field analysis or inversion. Knowledge of the direction of a magnetisation is more valuable if there are other magnetisations in the area with which it can be compared

5.3 RESULTANT (REMANENT AND INDUCED) MAGNETISATIONS

Two alternative descriptions of three-dimensional vectors are provided by the amplitudes of three orthogonal components (e.g. north, east and down) or by amplitude with declination and inclination angles. Figure 5.3 shows identical descriptions of the magnetic field and

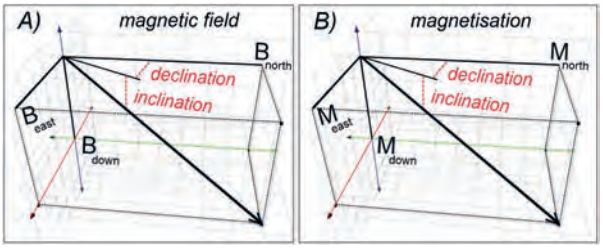

Fig. 5.3. Identical vector component and magnetisation direction (declination, inclination) descriptions of A) the geomagnetic field and B) magnetisation.

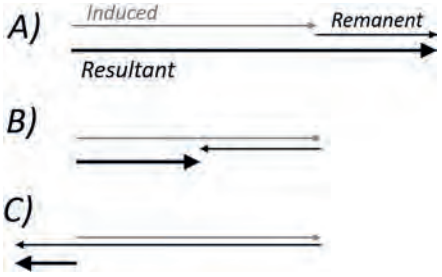

Fig. 5.4. Induced and remanent magnetisation vectors: A) parallel, B) anti-parallel (induced > remanent), C) anti-parallel (remanent > induced).

magnetisation in these two formats. If a magnetisation is purely induced with no anisotropy or self-demagnetisation effects then the declination and inclination angles of the magnetic field and magnetisation are identical.

As described in Chapter 1, magnetic field variations are expressions of contrast between magnetisations that are vector sums of induced and remanent components. Figure 5.4 shows the vector relationships for three of the four conditions in which induced and remanent magnetisation are either parallel or anti-parallel to each other. For parallel magnetisations (Fig. 5.4A) the amplitudes sum, with no rotation of direction. In static magnetic field surveys these magnetisations are indistinguishable from purely induced magnetisations of the same total strength.

Magnetisations that are closely anti-parallel exist in recent volcanic rocks that cooled during a period of reverse geomagnetic polarity. Surface and near-surface volcanic units that commonly carry these magnetisations have significant expression in magnetic field data (even if they are of small volume). Figure 5.4B represents the case that remanent magnetisation is weaker than the induced magnetisation (the Koenigsberger ratio is less than 1) and for which case resultant magnetisation is anti-parallel to the induced magnetisation. If the reverse remanent magnetisation is stronger than the induced magnetisation there is a 180° rotation of the resultant magnetisation direction as represented in Fig. 5.4C. If the strength of the remanent magnetisation only just exceeds the induced magnetisation the resultant intensity is low, but for Koenigsberger ratios of more than 2 it exceeds the strength of the induced magnetisation. Some volcanic episodes span both normal and reverse periods of the geomagnetic field with one or more reversals of the field, and these rock units may contain magnetic field expressions of mixed normal and reverse polarity. The fourth case not shown in Fig. 5.4 is that normal and reverse components have identical strengths and their resultant is zero.

Older rocks carry remanent magnetisations different in direction from the present geomagnetic field because of rotation by either post-intrusion tectonics or translation with continental drift. This leads to a much wider range of magnetisation directions. Induced, remanent and resultant magnetisations are co-planar and lie on a great circle in a stereographic projection. Figure 5.5A shows the relationship between these vectors for a Koenigsberger ratio less than 1 and Fig. 5.5B for a Koenigsberger ratio greater than 1. The Koenigsberger ratio is a scalar measure and does not completely describe the vector relationship between induced and remanent magnetisation. It cannot be determined directly from magnetic field data and therefore is of limited application in magnetic field analysis. For analysis of magnetisation direction recovered from magnetic field data the Koenigsberger ratio should be augmented with the apparent rotation angle (ARRA) between induced and resultant magnetisations that can be recovered directly from analysis or inversion of magnetic field

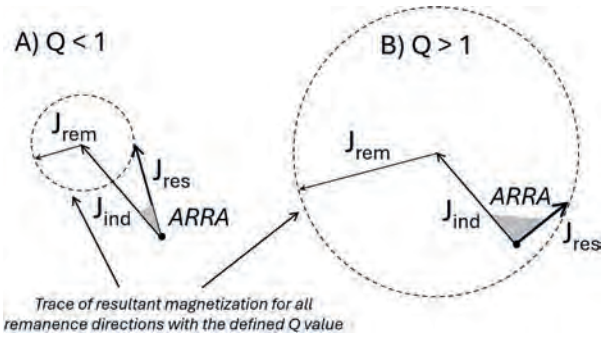

Fig. 5.5. Coplanar induced (Jind), remanent (Jrem) and resultant (Jres) magnetisations for A) Koenigsberger ratio (Q) > 1 and B) Q > 1. The apparent resultant rotation angle (ARRA) is between induced and resultant magnetisation vectors.

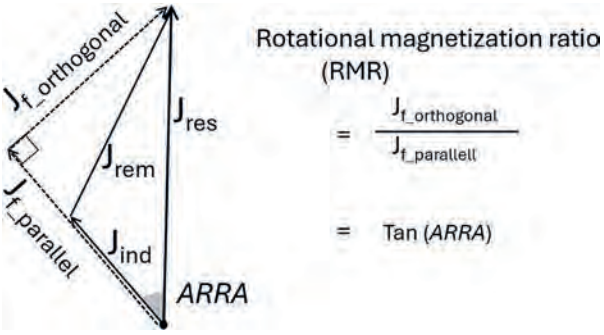

Fig. 5.6. Classification of magnetisation from magnetic field analysis as field-parallel (Jf_parallel) and field-perpendicular (Jf_orthogonal) components rather than laboratory classification as induced (Jind) and remanent (Jrem) magnetisations.

data. In Fig. 5.5 the trace of the resultant magnetisation vector for different directions of remanent magnetisation is mapped by the dashed circles. If the Koenigsberger ratio is less than 1 (Fig. 5.5A) there is a limited range for the resultant direction. If the Koenigsberger ratio is greater than 1 (Fig. 5.5B) the resultant can lie anywhere along the great circle that includes the induced and resultant magnetisation directions. Only if magnetic susceptibility is known or the Koenigsberger ratio is assumed can the remanent magnetisation strength and direction be found by completing the vector triangle.

Splitting a magnetisation into induced and remanent contributions is consistent with its genesis and provides a direction for the remanent magnetisation that should have geological meaning, but this cannot be done from magnetic field data alone. For magnetic field analysis, as shown in Fig. 5.6, a more practical separation of the magnetisation is in terms of the component parallel to the field that includes induced magnetisation with addition or subtraction of the parallel remanent contribution, and the remanent component perpendicular to the field (that can only be due to remanent magnetisation). The ratio of these components is given by the tangent of the ARRA angle, from which a maximum bound can be placed on the Koenigsberger ratio.

5.4 RECOGNITION OF MAGNETISATION DIRECTION IN MAGNETIC FIELD IMAGERY

Visual detection of differently directed magnetisations in magnetic field imagery provides a starting point for their analysis. If the field variations all appear to be consistent with magnetisations parallel to the geomagnetic field then a standard analysis can proceed. For instance, reduction-to-pole (RTP) transforms can be applied with limited concern of distortion by inappropriate magnetisation direction. If any of the magnetic field variations appear to be inconsistent with field-parallel magnetisation then two different approaches to their analysis are to minimise the influence of magnetisation direction by applying a total gradient or NSS transform to the data, or to highlight influence of magnetisation direction by submitting those features to a dedicated analysis or inversion to determine their magnetisation direction.

Figure 5.7 shows alternative images of a TMI grid measured in a geomagnetic inclination −60°, declination 0°. Sun-shading is a popular magnetic field display option designed to accentuate subtle, low-amplitude features. Figure 5.7.A is an image with subdued sun-shading and Fig. 5.7.B is a 'flat' image without sun-shading and with a contour overlay to indicate the true amplitude variations. Both images have a common histogram-equalised colour stretch (the colour scale is adjusted so that each colour is assigned to an equal area). This reveals maximum detail across the image (commonly applied to adress the highly dynamic range of magnetic field data that includes values substantially higher and substantially lower than mot of the data) but even by reference to a colour scale bar it is difficult to evaluate the absolute amplitude range of individual features. The discrete anomalies scattered across the map area have three different magnetisation directions (labelled 'a' to 'c' in Fig. 5.7.B). The different anomaly patterns caused by these three magnetisations are quite subtle in Fig. 5.7.A but with the help of the contour overlay are more easily discriminated in Fig. 5.7.B. Recognition of these differences in magnetisation may be critical to the magnetic field interpretation if, for instance, known mineralisation is associated with one direction whereas the other directions are association with barren bodies, or if the different magnetisations indicate different ages of the source bodies. Note that for the smooth background field of Fig. 5.7 in which the discrete anomalies produce the sharpest field gradients, the anomaly patterns can also be effectively highlighted by application of a vertical derivative filter that preferentially expresses the local anomalies and supresses longer wavelength gradients in the background field. A sound approach to magnetic field interpretation is to start with piecewise inspection of each discrete feature to best determine the information it carries, and then to proceed to relate those features in a geological synthesis.

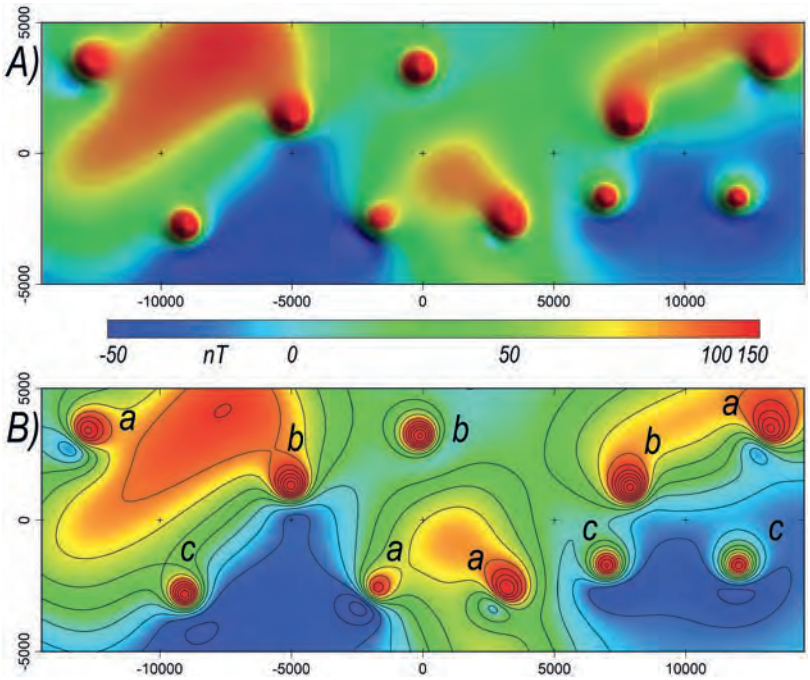

Fig. 5.7. TMI A) with north-east sun-shading, B) with 20 nT contours. Magnetisations: a) inclination −20°, declination 40°, b) inclination −80°, declination 300°, a) inclination −60°, declination 0°.

5.5 EXPRESSION OF MAGNETISATION IN PROXIMAL AND DISTAL FIELDS

Chapter 6 illustrates the influence of position, shape and plunge of a magnetisation on its magnetic field expression and the trade-offs arising in compensation by these factors for any errors in estimation of magnetisation direction. The influence of shape and plunge are most pronounced in a proximal magnetic field immediately surrounding a magnetisation and these influences attenuate in more distal fields. Figure 5.8 shows central north–south profiles over horizontally co-centred spherical and ellipsoidal magnetisations with inclination −90° in a northerly directed magnetic field of inclination −60°. In Fig. 5.8A TMI is computed at an elevation 100 m above the tops of ellipsoidal magnetisations and 340 m above the top of a spherical magnetisation of identical volume. All bodies have identical vertical magnetisations of intensity 1 A/m. The ellipsoids have a long axis of 400 m radius and the other two axes of 100 m radius, with dips vertical and at 45° to north and south. All four curves have different shape. The horizontal locations of the anomaly peaks for the sphere and vertical ellipsoid are co-located close to the centre of magnetisation, but over the plunging ellipsoids there is considerable horizontal offset of the anomaly peaks in the up-plunge direction. Figure 5.8B shows the curves computed 400 m higher. This is an increase in height by a factor of 5 from the shallowest magnetisations of the three ellipsoids. The increase in elevation causes substantial reduction in amplitude of the computed fields as shown by the solid-line profiles in Fig. 5.8B. To more easily compare these curves the magnetisation intensities were increased to normalise all curves to a peak of 100 nT as shown by the dashed-line profiles. The horizontal displacements between the peaks of the various curves are reduced substantially with the increase in elevation of the computed field, and the curves have more consistent pattern (the anomaly pattern is less revealing of plunge). The curves of the three ellipsoids could be brought to a closer match by applying slight horizontal displacements to counteract the bias introduced by differences in horizontal location of their shallowest magnetisations. If the fields were computed at even higher elevations, the amplitudes of the curves would weaken further and the shape and position of the curves would converge more closely. At extreme elevations all four bodies would produce near-identical (very low amplitude) field variations, and in each case inversion of those anomalies should use a spherical (dipole) model because there would be no justification to represent any apparent axial elongation or plunge that had little or no influence on the computed magnetic field.

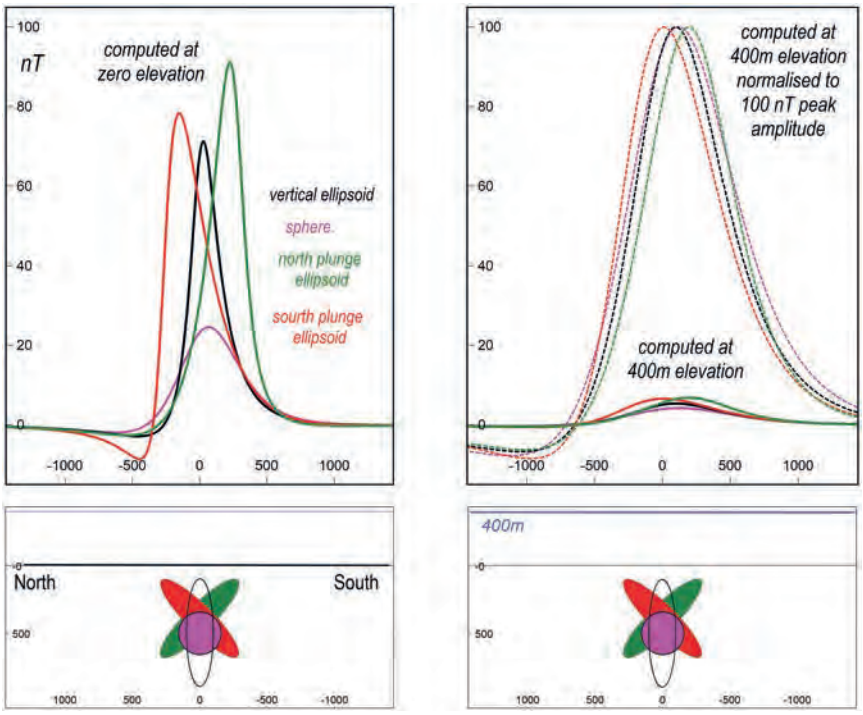

Fig. 5.8. North–south central profiles over horizontally co-centred sphere and ellipsoid magnetisations computed at A) 100 m above tops of the ellipsoid bodies and B) 500 m above the tops of the ellipsoid bodies.

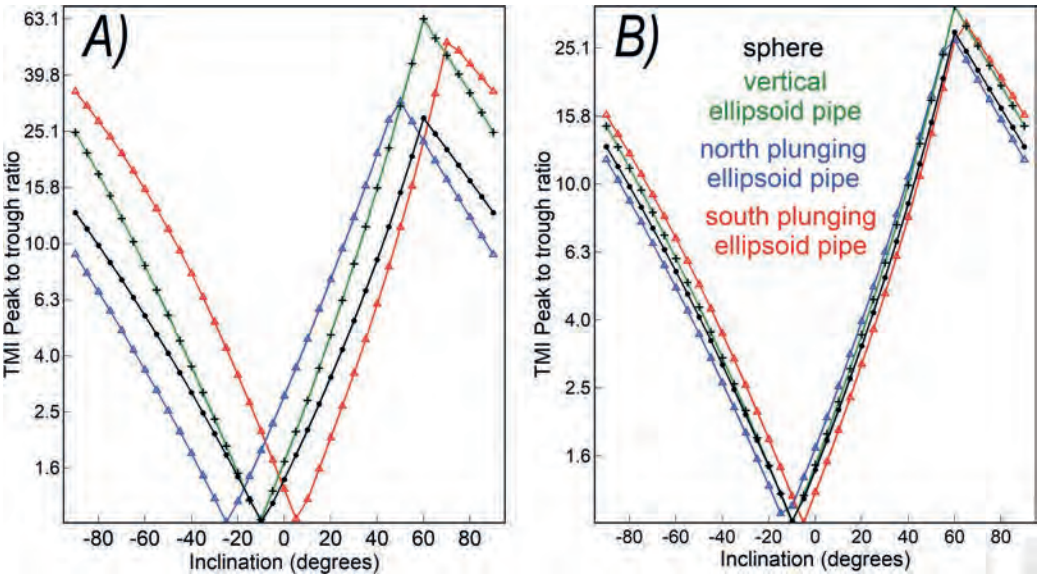

Fig. 5.9. Peak to trough amplitude ratios for the bodies shown in Fig. 5.6 and computed at the same lower elevation A) and higher elevation B) for north–south magnetisations with inclinations −90° to +90°.

Figure 5.9 plots peak-to-trough ratios for the four bodies shown in Fig. 5.8 at the two different field elevations and computed for the complete range of inclinations of magnetisation from −90° to +90°. On a logarithmic amplitude scale the curves can be split into approximately straight-line segments convenient for prediction of inclination of magnetisation from measurement of the anomaly peak and trough amplitudes. For the lower elevation measurements (Fig. 5.9A) curves for the different models form a wide band and recovery

of the angle of inclination of magnetisation would require knowledge or independent determination of its plunge. At the higher elevation (Fig. 5.9B) the influence of plunge of the magnetisation is greatly reduced and would supply only a fine-tuning in estimation of the inclination angle by up to ~5°. As explained in Chapter 14, an improved estimate of inclination of magnetisation from the peak to trough amplitude ratio of a magnetic field anomaly can be achieved after application of a transform to provide the vertical component of the field B_z or its vertical derivative $B_{z,z}$.

5.6 RTP TRANSFORM OF FIELDS DUE TO REMANENT MAGNETISATION

The reduction to pole (RTP) transform is widely used in magnetic field interpretation to compensate for inclination effects of the geomagnetic field and approximately centre magnetic field variations over their source magnetisations (Baranov and Naudy 1964; Blakely 1995). The transform has limited influence in steep geomagnetic inclinations and has instability issues when applied to low inclination fields. The RTP applies phase transforms to bring the geomagnetic field and the source magnetisation to vertical. A standard RTP transform assumes that the initial magnetisation is parallel to the local geomagnetic field but this can be amended for magnetisations of different known direction. RTP with a different input magnetisation direction is generally restricted to single anomalies because it is unusual to have multiple magnetic field variations directed consistently other than parallel to the geomagnetic field. Before applying an RTP transform it is important to carefully inspect the TMI image using the cues described in section 5.4 to recognise magnetic field expression of magnetisation direction. It is more difficult to later recognise the expression of magnetisation direction in the output of an RTP that has already been applied. Trial application of RTP with different magnetisation directions has been shown capable of recovering magnetisation direction by cross-correlation with a transform such as the total gradient that approximately centres field variation over a magnetisation similarly to a successful RTP (Dannemiller and Li 2006). There have also been associated attempts to estimate magnetisation direction by correlation of gravity and transformed magnetic fields; however, geological complexity and limited correlation of density and magnetisation contrasts generally restricts this analysis (see Chapter 1).

Figure 5.10A shows the TMI Black Hill Norite north-west anomaly and Fig. 5.10B shows a standard RTP transform using the assumption of magnetisation parallel to the geomagnetic field. The background field has a relatively steep inclination of −67° and the standard RTP creates only a minor adjustment and southerly displacement of the anomaly. Figure 5.11 shows parametric inversion of the anomaly with a polygonal sheet model using Modellvision software (Foss and McKenzie 2011). The free parameters are the location of the model, its size and shape (defined by vertex coordinates), depth to the top, depth extent, plunge, resultant magnetisation intensity and direction. The best-estimated magnetisation has intensity 39 A/m, declination 232° and inclination +8°. Figure 5.12 shows the output of an RTP transform using the inversion-estimated magnetisation direction. This produces a compact, almost positive-only anomaly consistent with expectation of an anomaly in a vertical geomagnetic field over a compact vertical

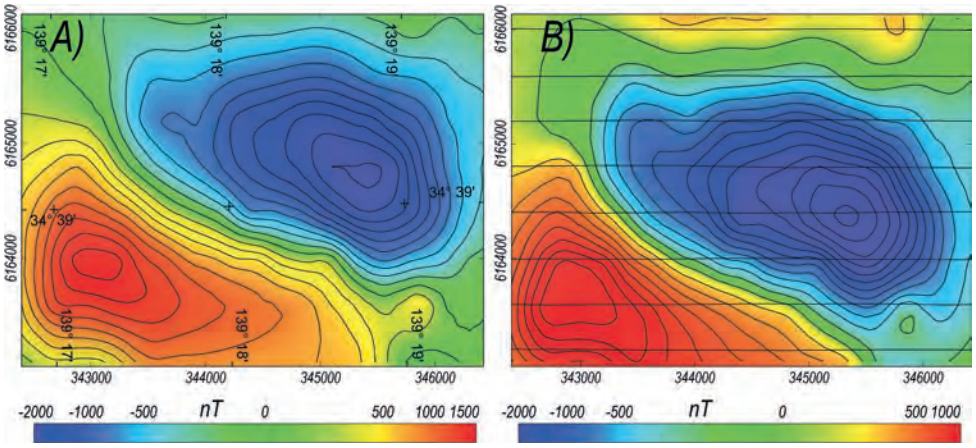

Fig. 5.10. Black Hill Norite north-west anomaly A) TMI and B) standard (induced magnetisation) RTP.

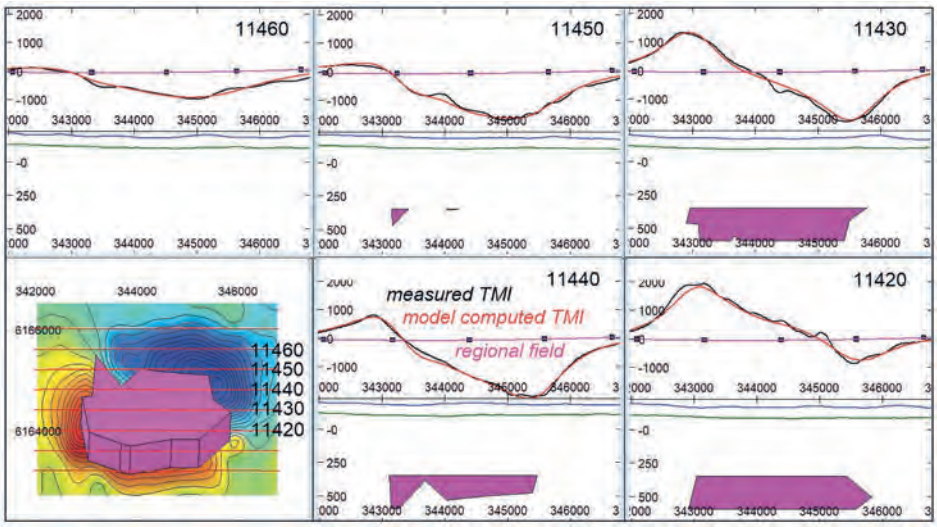

Fig. 5.11. Black Hill Norite north-west anomaly inversion model sections. Model magnetisation intensity 39 A/m, declination 232°, inclination +8°.

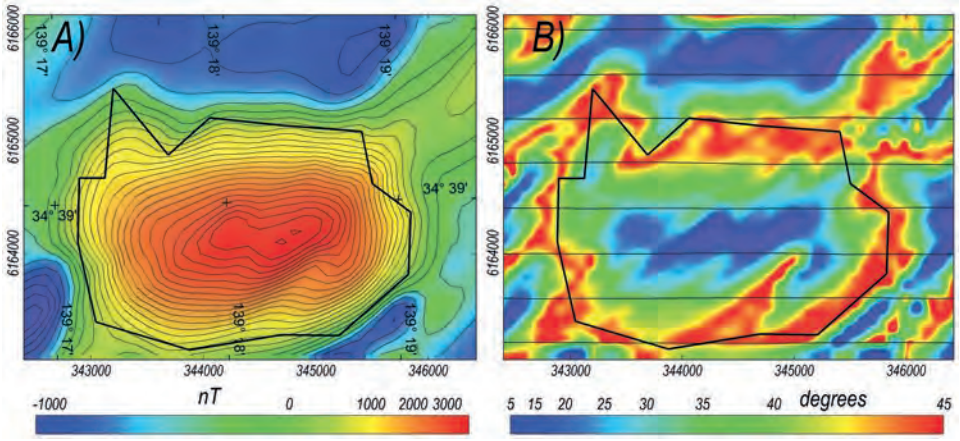

Fig. 5.12. Black Hill Norite north-west anomaly A) RTP using the inversion resultant magnetisation direction, with an overlay of the edge of the inversion model and B) edge inversion of the RTP anomaly.

magnetisation. The RTP anomaly location and shape is also consistent with the inversion model as shown by the trace of the model outline on the RTP image in Fig. 5.12A, and on an edge filter transform of the anomaly in Fig. 5.12B (from Foss and McKenzie 2011). This correspondence does not prove the transform correct because it is derived with input from the inversion model, but the close agreement is strong support for both the estimated magnetisation direction and the spatial model. While the standard RTP transform using an induced direction magnetisation (a rotation of 23° to the vertical) generated only a modest change to TMI (Fig. 5.10B), RTP with the estimated resultant magnetisation direction (a rotation of 82° to the vertical) produced the radically different RTP output (Fig. 5.12A). In this case the substantial rotation of the sub-horizontal magnetisation direction to vertical is clearly more significant in the RTP process than the slight change in magnetic field direction.

Foss *et al.* (2021) performed an analogue model test of the RTP of the Black Hill Norite north-west anomaly. A palaeomagnetic rock core of the Black Hill Norite itself (a cylinder with height 2.5 cm and radius 2.5 cm) was given a saturation magnetisation along its axis and placed in a Rubens cage (Fig. 5.13) oriented to replicate the low-inclination south-west directed resultant magnetisation of the Black Hill Norite, with the applied field set to the direction at the Black Hill Norite site. The magnetic field was measured with a three-component magnetometer drawn along 'flightlines' with the sample sequentially moved perpendicular to the flightlines to generate the survey. Individual flightline data were levelled to replicate what would normally be achieved with

Fig. 5.13. Rubens cage in which the magnetometer was run along the yellow track above the rock cylinder sample carrying a magnetisation in the Black Hill Norite direction. The background field was set to be identical to the geomagnetic field at the Black Hill Norite location. The survey was performed by moving the sample perpendicular to the track after recording each flightline.

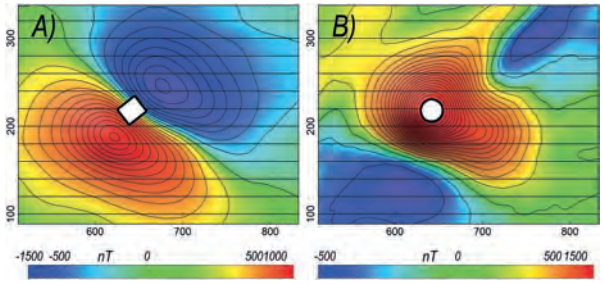

Fig. 5.14. TMI maps from surveys in the Rubens cage emulating A) the Black Hill Norite north-west anomaly and B) the RTP anomaly created by rotating the magnetisation to a vertical direction and setting the background field to vertical.

tie-line levelling and then residual misfits were attenuated with micro-levelling. The resulting TMI image (Fig. 5.14A) closely matches the measured Black Hill Norite north-west anomaly (Fig. 5.10A) revealing that for this anomaly, magnetisation direction is much more influential in determining anomaly shape than the distribution of magnetisation. An analogue RTP (Fig. 5.14B) was performed by repeating the Rubens cage survey with the core rotated to have a vertical magnetisation and the background field set to vertical. The measured field of this 'polar' survey is an almost positive-only anomaly consistent with that expected from a successful RTP transform. RTP of both the measured Black Hill Norite TMI anomaly and the synthetic anomaly generated in the Rubens cage using the same input magnetisation direction were successful, but both show striations parallel to the magnetisation direction. These striations are attributed to distortion caused by the low inclination of magnetisation (Foss *et al.* 2021). The analogue experiment reinforces the substantial influence of magnetisation direction and the validity of including it in the RTP transform.

Well-known instability of the RTP transform for low-inclination magnetic fields (Blakely 1995) arises from extreme amplification of what should be near-zero terms. The synthetic Black Hill Norite Anomaly experiment demonstrates that this instability also applies to RTP transform of low-inclination magnetisation in high-inclination fields. At any given geomagnetic inclination, RTP transform of reliable TMI data should be stable but instabilities are introduced for noisy data, data with errors such as levelling busts or incorrect representation by gridding because the flightlines are too widely spaced.

The RTP transform does not substantially change the power spectrum of the data. Long wavelength components of the field (generally due to deeper magnetisations) have the greatest displacement and should move towards the pole. RTP transform of TMI grids with substantial north–south variation in the background field can be problematic. In these cases it is especially important that the data are well padded to a considerable distance beyond the grid border (preferably by including the true field data in that region). Note that for small survey areas and deep magnetisations, the measured magnetic field may not have any influence from the magnetisation directly beneath the survey area.

5.7 INVERSION OF HORIZONTALLY COMPACT, STEEPLY PLUNGING ('PIPE') MAGNETISATIONS

The key trade-off against error in assigned magnetisation direction is the horizontal location assigned to a magnetisation. However, for a magnetic field measured closely above a magnetisation, horizontal position is effectively locked in place. Dominance of the influence of the shallowest section of a magnetisation reduces the confidence with which deeper sections can be investigated by magnetic field analysis or inversion. In consequence of these relationships, an effective compensation for error in magnetisation direction is horizontal misplacement of magnetisation at depth in the form of an incorrect apparent plunge. Even if a magnetisation does not have significant extension to depth, inversion can create apparent extension. If a body is elongate in one horizontal direction (a sheet-like body) the compensation

by apparent plunge is quite effective and neither plunge nor magnetisation direction can be reliably estimated. For a body that is horizontally compact (for instance a pipe) compensation for error in magnetisation direction by an erroneous apparent plunge still applies but is less effective.

We know that inversion solutions are non-unique and that close fits to measured data do not necessarily qualify an inversion model as a reliable representation of the true magnetisation. Even allowing for this uncertainty, the only practical measure that we have for acceptance of an inversion model (excluding highly interpretive geological appraisal) is the goodness of fit between its computed magnetic field and the measured magnetic field, and the most reliable result of inversion is exclusion of models that produce unacceptable data misfits. In practice, discomfort in acceptance of an inversion model increases gradually with increasing data misfit but there is no diagnostic test of whether a model should be accepted or rejected. Data misfit is often either the only factor or the major factor by which a model is evaluated and is commonly the key or sole driving factor in its inversion. To better understand inversion we can investigate success in recovering known models from inversion of the fields forward computed from them, starting with an inappropriate model and tracking its (hopefully progressive) return to the input model as inversion reduces the data misfit.

Figure 5.15 is a schematic of the inversion process. A starting model is shown in the top left of the figure where it has both a large data misfit and a poor representation of the true magnetisation. In this study I measure success of an inversion by the spatial overlap of the model with the known magnetisation. With the objective of reducing data misfit, inversion can only proceed in a downward direction in Fig. 5.15. If the model change is directly downwards then the inversion does not improve the model but only reduces the discrimination for any subsequent inversion that will start with a smaller data misfit. The ideal of inversion is that the reduced data misfit is achieved by true improvements to the model, in which case the inversion proceeds diagonally downwards and to the right towards a model that is a closer representation of the ground and has a low data misfit as a consequence of this.

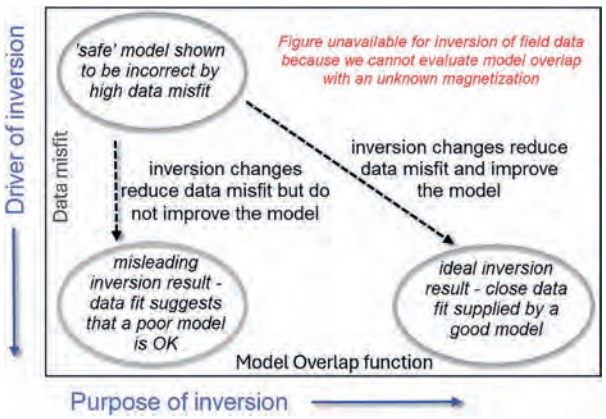

Fig. 5.15. Schematic of the relationship between the objective function of an inversion to reduce data misfit and the purpose of inversion to better represent the source magnetisation.

Figure 5.16 shows north–south and east–west profiles through the centre of an equidimensional anomaly due to a vertical pipe with induced magnetisation in a north–south geomagnetic field of inclination −60°. The complete anomaly from which these profiles have been extracted was inverted with models of an induced magnetisation sphere and ellipsoid. The data misfit of these models is because they have inappropriate geometries (different to the input pipe model). The spherical model is simpler than the ellipsoid model, has a larger data misfit and a smaller overlap with the input model. The data misfit of the spherical model might be recognised to betray a significant misrepresentation of the true magnetisation, and that might be the incentive to attempt inversion with the more complex, ellipsoidal model. It is unlikely for measured field data and a geological source body that meaning would be assigned to the residual data misfit as small as that of the ellipsoidal model, but the input model is already reasonably represented (other than for the detail of depth to its top). The

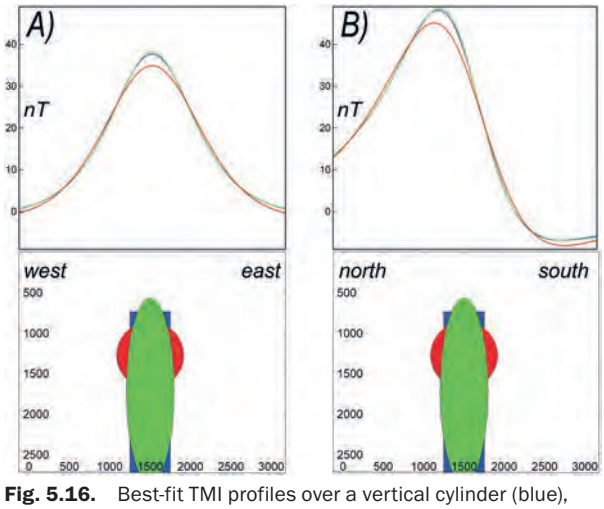

Fig. 5.16. Best-fit TMI profiles over a vertical cylinder (blue), spherical inversion model (red) and ellipsoid inversion model (green). A) east–west and B) north–south. All bodies have magnetic susceptibility 0.05 SI.

progression of an inversion from the spherical to the ellipsoidal model represents a productive inversion as a move downwards and towards the right in Fig. 5.15.

Following the simple case of Fig. 5.16 we can proceed to the more complex situation that the input vertical pipe model has a magnetisation differently directed to the magnetic field but that inversion is forced to proceed on the assumption that magnetisation is induced. Figure 5.17 shows TMI computed from three vertical pipe models with magnetisations divergent by 30° from the geomagnetic field direction of inclination −60°. The pipes have radii of 100 m, depth extents of 2000 m and the field is computed 150 m above their tops. The westernmost pipe has a steeper magnetisation of inclination −90°, the central pipe has an eastward rotation of magnetisation of declination 62.35° and the easternmost pipe has a shallower magnetisation of inclination −30°. From visual inspection of this ideal computed data it should be evident that the magnetisations are likely to be differently directed to the magnetic field and inversion should allow for that. However, with irregularities of measured survey data and widespread reluctance to introduce complexities of remanent magnetisation, many anomalies such as these are inverted on the assumption of induced-only magnetisation.

Figure 5.18 shows a perspective view of models produced by different inversions of the anomalies imaged in Fig. 5.17. The input vertical circular-section pipe models with rotated magnetisations are shown in magenta. Inversions using spherical models with free magnetisation direction generated the bodies shown in red in Figs 5.18 and 5.19. The spheres are horizontally co-centred with the source magnetisations and recover their magnetisation directions faithfully. The relationship between these spheres and the input pipe magnetisations is identical to that between the induced-magnetisation sphere and pipe in Fig. 5.16. Inversions for magnetisations with known vertical plunge have no penalty from allowing a free magnetisation direction. However, if inversion forces an induced magnetisation (a direction 30° different to the true magnetisation direction for all three anomalies in Fig. 5.17) spherical models are horizontally displaced from the input magnetisations as shown by the light blue spheres in Figs 5.18 and 5.19.

Inversions using models assumed to have the same induced magnetisation but as vertically extended pipes produce the bodies shown in green in Figs 5.18 and 5.19 that are horizontally co-located with the induced magnetisation spherical models. This demonstrates that magnetisation direction is more effective than details of shape in estimation of the horizontal position of a magnetisation. The induced magnetisation spherical and vertical pipe models have large data misfits that should reveal that they are inappropriate models.

Inversions can also allow the magnetisation to plunge (adding two free inversion parameters of plunge angle and azimuth). In Figs 5.18 and 5.19 plunging induced magnetisation pipe models are shown in dark blue. To compensate for the 30° error in magnetisation direction that is too steep, horizontally rotated or too shallow, the models develop plunges from the vertical of 31°, 30° and 27° respectively with azimuths that vary systematically with input magnetisation direction as shown in Figs 5.18 and 5.19. In compensation for the input magnetisation that is too steep the plunge azimuth is towards the pole (to the south for this southern hemisphere example); for

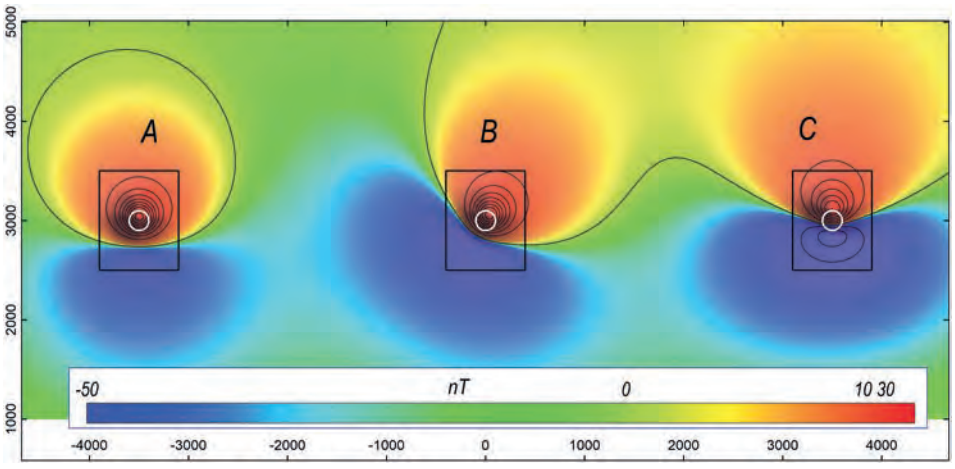

Fig. 5.17. TMI anomalies over vertical cylinders: A) inclination −90°, B) inclination −60°, declination 62°, C) inclination −30°, declination 0°. The background field has declination 0°, inclination −60°.

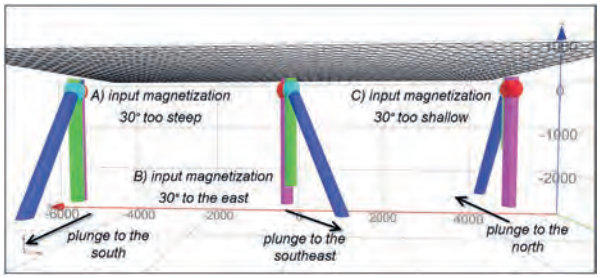

Fig. 5.18. Input remanently magnetised vertical pipes (magenta) and inversion models: free magnetisation spheres (red), induced spheres (light blue), induced magnetisation vertical pipes (green) and induced magnetisation plunging pipes (dark blue).

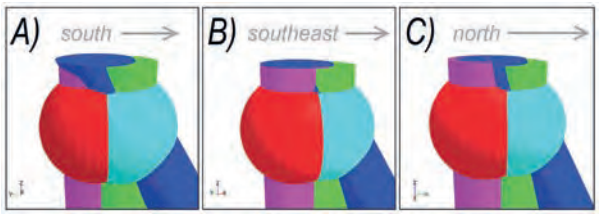

Fig. 5.19. Detail of the tops of the models shown in Fig. 5.18 that highlight the systematic influence of error in magnetisation direction and model geometry. Each view is perpendicular to the plunging induced magnetisation models (shown in dark blue).

the input easterly directed magnetisation the plunge is to the south-east; and for the input magnetisation that is too shallow the plunge is away from the pole (in this case to the north). Figure 5.19 shows the input and inversion models in perspective views perpendicular to the plunge of the induced pipes and illustrates the consistent effect of the magnetisation errors, with offset of the induced spheres and vertical pipes in the down-plunge direction. At this shallow measurement elevation the tops of the plunging pipes are approximately locked in place and the erroneous plunge takes the deeper sections of the inversion models progressively further from the true magnetisation. This reveals the weak concept of a centre-of-magnetisation for deep-going bodies. The base of the bodies contributes very little to the magnetic field variation and the magnetisation has a shallower effective centre-of-magnetisation than its true depth. The difference between effective and true centre of magnetisation depends on the elevation and nature of the measurements (whether they are of the field or its gradients). Shallower measurements and gradient measurements focus magnetic field analysis preferentially on the shallower sections of magnetisation.

Figure 5.20 shows contours of the magnetic field computed for the input vertical pipes with 30° rotated magnetisations (blue) and the inversion-derived

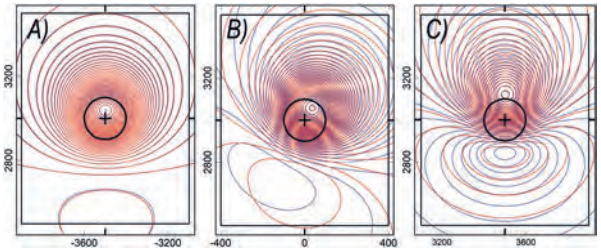

Fig. 5.20. Details of TMI in the areas outlined in Fig. 5.17: TMI contours (blue) of vertical pipes with magnetisations: A) declination 0° inclination −90°, B) declination 62.35° inclination −60° and C) declination 0° inclination −30° and (red) of best-fit plunging magnetisation pipes of declination 0°, inclination −60°. Circles show the edges of the vertical input models.

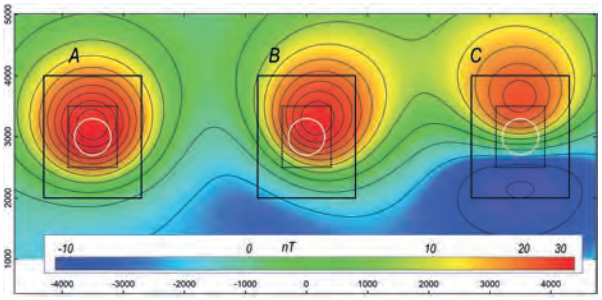

Fig. 5.21. The same magnetisations as in Fig. 5.17 (but in bodies three times wider) computed at an elevation of 1,000 m above the top of magnetisation. White circles show outlines of the input magnetisations. Dashed rectangles are extents of the previous shallow magnetisation studies and larger rectangles are the areas shown in Fig. 5.22.

plunging induced magnetisation pipes (red). The misfit between these fields is small and with even the best survey data it would not be feasible to attribute meaning to the residual data misfits, nor would those residual differences reliably drive further inversion changes to the model as they are smaller than would be anticipated from geological irregularities and data imperfections. The data misfit is least for the steeper magnetisation (Fig. 5.20A), meaning that model error is more readily accommodated for magnetisation directions that are too steep, and this provides a bias to inversion results.

Figure 5.21 shows the lower amplitude TMI field computed over deeper magnetisations with tops 1,000 m below the computation surface. The magnetisations are identical to the shallower bodies previously studied. Depth extents are the same but the pipes are wider (300 m radius) and volumes are nine times larger. Small and deep bodies are rarely detected reliably in magnetic field surveys unless they have extremely high magnetisation intensities. From images of this distal field it is more challenging to predict the horizontal location of the tops of the magnetisation (plotted as white circles in Fig. 5.21)

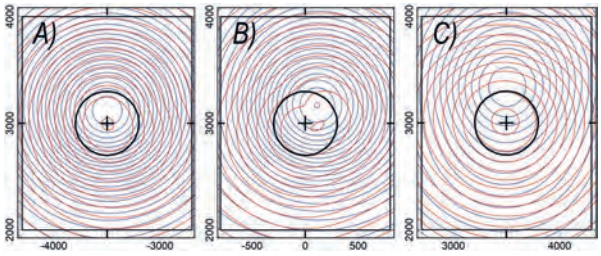

Fig. 5.22. Details of TG (blue) and NSS (red) contours computed from the TMI grid of Fig. 5.17. The black circles are the magnetisation outlines. In all cases the NSS is superior to the TG in locating the magnetisation.

because the proportional influence of the shallowest magnetisation reduces with increased source depth. Enhancement transforms can be used to assist in locating source bodies irrespective of their magnetisation direction. Figure 5.22 shows contours of TG (blue) and NSS (red) with the centres and margins of the magnetisations marked by the black crosses and circles respectively. For all three magnetisation directions the NSS peak closely marks the centre of magnetisation (because the magnetisations have vertical plunge) but the TG transform performs less well. For the horizontally rotated magnetisation the TG peak is close to the edge of the magnetisation and for the shallow magnetisation it plots outside the magnetisation (these details vary with the geometry of the source magnetisation, its depth and magnetisation direction).

I performed the same series of inversions for these deep magnetisations as for the shallower magnetisations and evaluated performance of both sets of inversions using criteria as plotted schematically in Fig. 5.15. The data misfit for each inversion is measured as the standard deviation of the data misfit normalised to the standard deviation of the input data and converted to a percentage. The success of the inversion is measured as the product of overlap between the input and inversion models normalised to the volume of the input model (a measure of what proportion of the input model is correctly located) and the same overlap normalised to the inversion model volume (a measure of what proportion of the inversion model correctly locates magnetisation). This measure is also converted to a percentage. The second term (the proportion of the inversion model that correctly locates magnetisation) is required to discriminate against large volume inversion models that include the input magnetisation but have little value in localising it. Overlap volumes are computed only across the depth range of the top 10% of the input model. No significance should be ascribed to models beneath that depth. Deep-going magnetisations such as those investigated here are almost invariably tested by drilling only in their shallow sections. It is unlikely that bodies of depth extent 2,000 m such as these would be drilled to depths of more than 200 m below their tops, and even if they were to be, it is evident that the inversion models do not provide reliable guidance to those depths because the shallower sections of magnetisation completely dominate the measured magnetic field variations. As noted above, the induced magnetisation models with the lowest data misfit achieve that by a compensating plunge that takes their deeper sections further from the input magnetisation, with no overlap of those deeper sections.

Some of the key conclusions from the inversions are illustrated in Fig. 5.23 in cross-plots consistent with the inversion process schematic of Fig. 5.15. Figure 5.23A shows the results of the spherical model inversions. The spheres were restricted to have intensity of magnetisation identical to the input magnetisation because there is no sensitivity to that parameter, only to its product with volume to give the magnetic moment. The spherical inversion model geometry is very different to the input magnetisation and this limits the possible overlap to no more than ~50% as plotted in Fig. 5.23A. In Figs 5.23 and 5.24 induced magnetisation inversion results are plotted with closed symbols and free magnetisation direction inversion results are plotted with open symbols. Shallow model results are plotted in blue and deep model results are plotted in red. At both depths the free magnetisation models produce the lower data misfits and have the larger overlap with the input magnetisation, qualifying inclusion of the free variable of magnetisation direction as a successful inversion strategy. As already noted, these output models are centred on the axis of the input magnetisation, whereas the induced magnetisation inversion models are off-centred.

Figure 5.23B shows the influence of allowing free plunge in the induced-magnetisation-only inversions. The vertical inversion models (the triangular symbols in Fig. 5.23B) are compatible with the vertical input magnetisation but are offset because of their incorrect magnetisation direction. At both depths, freedom of plunge allows the inversion to reduce data misfit (as shown by the square symbols). For the shallow models there is significant reduction of data misfit but almost no increase in overlap resulting from inversion with free plunge. These are ineffective inversions (although that would not be known for inversions with unknown

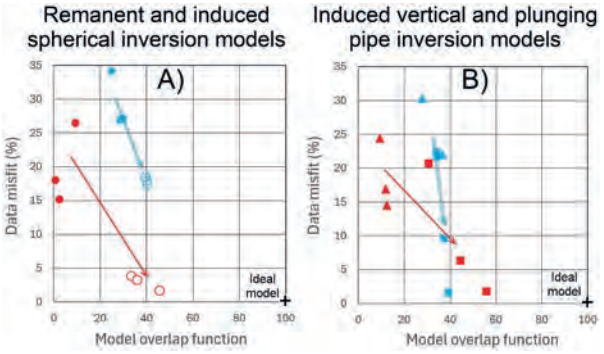

Fig. 5.23. Data misfit against model overlap for inversions with A) induced and remanent spherical models and B) induced vertical and plunging pipe models. Symbols are explained in the text.

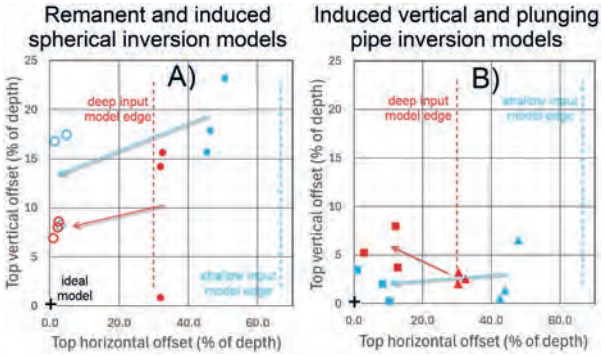

Fig. 5.24. Vertical and horizontal offsets for A) induced and free-magnetisation spherical inversions and B) vertical and plunging pipe induced magnetisation inversions. Symbols are as in Fig. 5.23.

sources). For the deep models the reduction of data misfit on allowing the magnetisation to plunge gives rise to an increase in overlap with the top 10% of the input magnetisation, but only to about twice that of the induced magnetisation spherical models and similar to the free-magnetisation spherical models. Note that in Fig. 5.23B inversion of this ideal synthetic data with a free-magnetisation pipe model would recover a model with a very high overlap.

Figure 5.24 shows horizontal misfit between input magnetisations and inversion models cross-plotted against vertical misfit. Horizontal misfit is measured between input magnetisation axes with spherical model centres in Fig. 5.24A and with top-face centres of pipes in Fig. 5.24B. Vertical misfit is measured between the top of input magnetisation and the top of the inversion models. Both the horizontal and vertical offsets are measured as percentages of depth to the top of the input magnetisation. Note that in Fig. 5.24 the ideal model (zero horizontal and vertical misfit) is plotted in the bottom left corner rather than the bottom right corner in Fig. 5.23.

The most significant differences between offsets of the spherical inversion models in Fig. 5.24 are between the small horizontal offsets of the free-magnetisation inversion models and the much larger horizontal offsets of the induced magnetisation inversion models. The free-magnetisation inversion bodies all have horizontal offsets of less than 5% but the centres of the deep induced-magnetisation inversion bodies lie just outside the extent of the source magnetisations. The vertical misfits for the spherical inversion models of Fig. 5.24A are similar for induced and free-magnetisation inversions, and both sets of inversions show a reduction in depth-weighted vertical misfit by ~50% between the shallow and deep models.

Figure 5.24B shows the results of induced magnetisation inversions with vertical pipes (triangular symbols) and plunging pipes (square symbols). All inversions have significantly less vertical misfit than for the spherical models in Fig. 5.24A. This emphasises the key importance of the shape of magnetisation in magnetic source depth estimation. Centres of the deep vertical pipe inversion models lie slightly beyond the margin of the input magnetisation (close to the centres of the spherical induced magnetisation models plotted in Fig. 5.24A). Including freedom of plunge in the inversions (the square symbols in Fig. 5.24B) reduces horizontal misfit of the top faces of 50% and 30% for the shallow and deep models respectively to only 10%. The spatial goodness of fit statistics of c. 10% horizontal offset and c. 6% vertical offset for the centre of the top face of the plunging induced magnetisation models in Fig. 5.24B present a more favourable report of the inversion results than the overlap measures for the same bodies of 30% to 60% over the shallowest 10% of the magnetisation as plotted in Fig. 5.23B. Note again that with pipe models, inversion of the noise-free synthetic data allowing freedom of magnetisation direction and an appropriate model type should achieve almost perfect representation of the input magnetisation.

5.8 A SENSITIVITY-EVALUATION CASE STUDY IN RECOVERY OF MAGNETISATION DIRECTION

Inversion applied to investigate unknown magnetisations are generally reviewed only according to data misfit. Verification of a model and evaluation of inversion errors comes only with any subsequent drilling. This case study reviews the sensitivity with which resultant

magnetisation direction and depth to magnetisation were recovered from inversion of a compact negative anomaly and the prediction of depth to magnetisation made in design of a drillhole. Figure 5.25A shows a negative TMI anomaly in south-west South Australia measured by the 2015 Coompana Survey (P1270) on seven east–west profiles at a ground clearance of 80 m. The anomaly has an approximate range of 820 nT, from 780 nT below the background level to 40 above it, although the anomaly separation is not well defined. Figure 5.25B shows the model-computed field resulting from a free-magnetisation inversion. Flightline model sections are shown in Fig. 5.26. The background field was given a near-linear west to east slope. Two independent inversions were performed, one using a horizontal-topped elliptic-section pipe (shown in red in Fig. 5.26) and one with a more versatile polygonal-section pipe (shown in blue in Fig. 5.26) for which the increased degrees of freedom achieve a marginally improved data-fit (only visually obvious on profile 30180 in Fig. 5.26). The two inversion models mostly overlap but have a difference in their top elevations of 40 m (13% of mean depth below sensor and 18% of mean depth below ground). Both bodies have similar widths and dips towards the east, with resultant magnetisation intensities and directions of 34 A/m, declination 1°, inclination +23° and 21 A/m, declination 2°, inclination +24° for the elliptic and polygonal section pipes respectively. For simplicity only the top of the ellipsoid model is plotted in the map views in Fig. 5.25. An RTP performed using the inversion-derived magnetisation direction produced the field imaged in Fig. 5.25C, that is almost exclusively a positive anomaly as expected of a successful RTP, with a peak coincident with the inversion model. The NSS transform of TMI is imaged in Fig. 5.25D. This image is independent of the inversion modelling but provides a very similar mapping of the horizontal distribution of magnetisation. Paine *et al*. (2001) used combined vertical integration and TG transforms (in both sequences) to invert TMI data with reduced sensitivity to magnetisation direction. Foss (2006) also used a transform image in staged inversion to approximately locate a source body, invert it for magnetisation direction, and then adjust both the spatial and magnetisation parameters in a final combined inversion (but found this approach unnecessary). Multiple synthetic and case studies have since established that provided the anomaly separation is appropriate and a reasonable starting model is used (guided if required by a suitable data transform) well-constrained inversion simultaneously resolves spatial and magnetisation parameters to give stable and reproducible solutions.

The estimated width of the top face of the polygonal section pipe inversion model is 190 m with an approximate length of 1100 m. Elongation of the body reduces confidence in the magnetisation direction estimate and the limited width of the body raises concerns that it might be missed with drilling. If the top of the body is narrowly missed in the up-dip direction the body will not be intersected, whereas if the top of the body is narrowly missed in the down-dip direction the borehole should still intersect it at a greater depth. Borehole CDP007 (Dutch *et al*. 2017a) into the source of this anomaly was designed with a westerly plunge based on the magnetic field inversion model results. This borehole

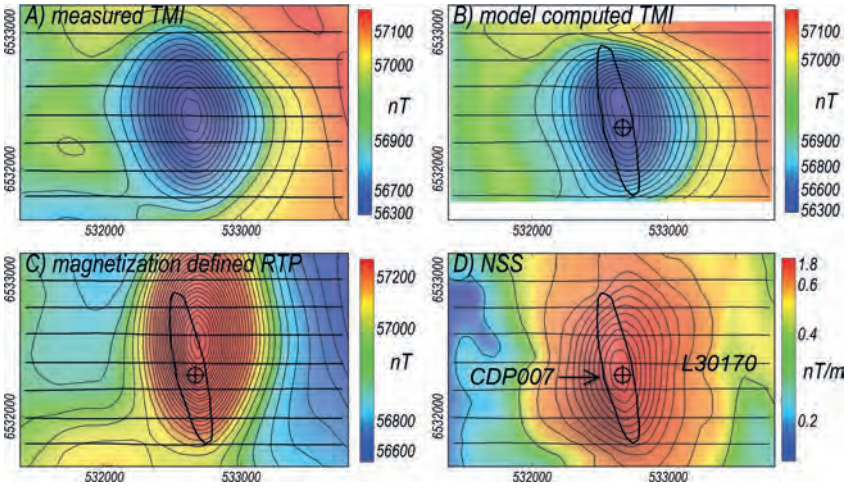

Fig. 5.25. Coompana ARAD anomaly 275: A) measured TMI, B) model-computed TMI, C) RTP derived with the supplied resultant magnetisation direction, D) NSS of TMI.

intersected the body within 10% of the depth below sensor of both inversion model predictions and at the horizontal location shown in the maps in Fig. 5.25. The borehole is also shown projected onto the nearest flightline section (line 30170) in Fig. 5.26.

Design of boreholes based on inversion studies benefits from understanding the confidence of those predictions. Non-uniqueness prevents a conventional measure of uncertainty in any inversion prediction but we can at least quantify the sensitivity of model-dependent estimations. We do this by first finding the model of a specified type that most closely fits the data (in a least-squares sense). This model is by definition the best combination of parameter values (including parameters of the background field) for that body type. Discovery of the parameter set is a multi-dimensional optimisation task, with each free parameter introducing an additional dimension. Sensitivity of the model to individual parameters is investigated by offsetting that parameter value and determining how effectively the resulting increase in data misfit can be compensated by revision of the other parameter values. In this study I investigated sensitivity to declination and inclination of magnetisation as well as to depth to the top of magnetisation. Figure 5.27 maps

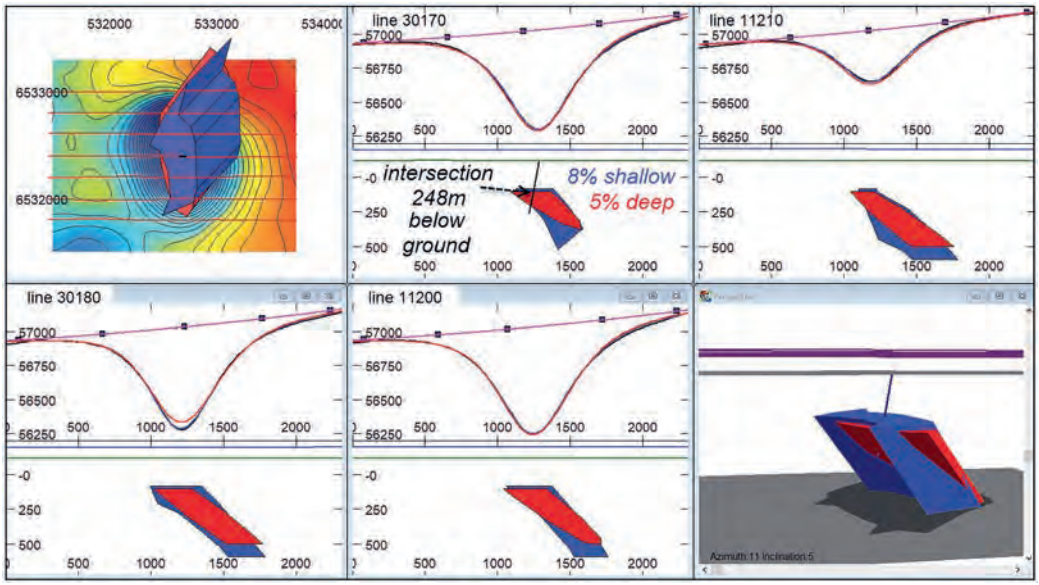

Fig. 5.26. Coompana ARAD anomaly 275 flightline model cross-sections with the elliptic pipe (red) and polygonal pipe (blue) models and their computed fields in the same colours. The magenta curve is the assigned background field.

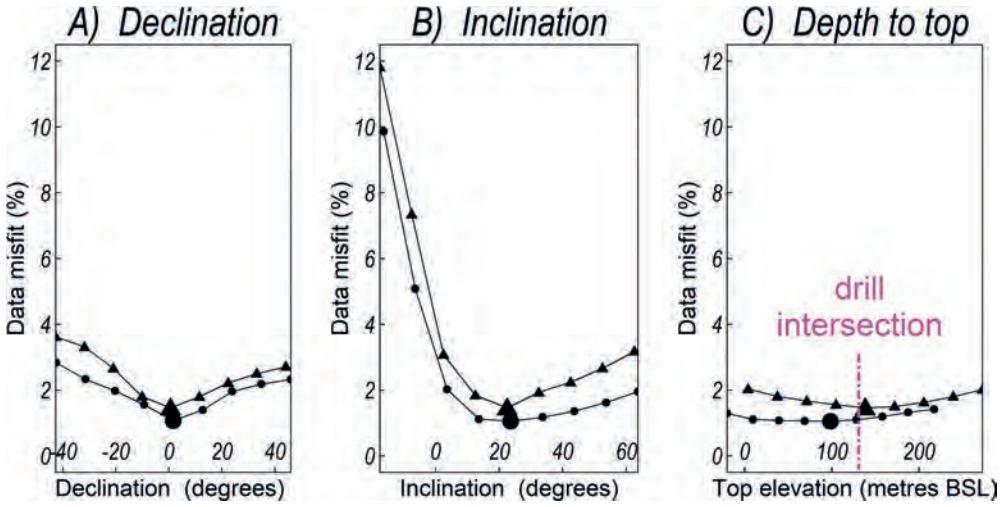

Fig. 5.27. Sensitivity curves for A) declination of magnetisation, B) inclination of magnetisation and C) depth to the top of magnetisation.

the increase in data misfit as those parameters progressively diverge from their values in the optimum parameter assemblage. The solutions determined by inversion to have minimum data misfits for the elliptic and polygonal section pipes (hopefully the global minimum solutions for those bodies) have misfit values (percentage standard deviation of the misfit normalised by standard deviation of the input data) of 1.1% and 1.5% respectively. These values represent field variations too complex or for some other reason unsuitable for explanation by a combination of background and model fields in the selection searched by the inversion. The absolute value of a residual data misfit does not have specific interpretational meaning, although large values raise questions about the suitability of proposed models to explain those field variations.

In Figs 5.27A and 5.27B misfit values are plotted for declination and inclination of magnetisation across a range of angles in steps of 10° about the optimum values. For the more complex polygonal-section pipes the values are plotted with circular symbols and for the elliptic-section pipes the values are plotted with triangular symbols. The difference in best estimated declination and inclination values between the two bodies are in both cases only 1°, although the error misfit curves in Fig. 5.27 suggests that these angles should not be interpreted to resolutions less than 5° to 10°. The section of the curves illustrating underestimation of inclination indicates a much greater sensitivity to this error than overestimation of inclination or error in declination. This is consistent with the synthetic data analysis in section 5.7. I also performed a sensitivity analysis of depth to the top of the magnetisation models in steps of 30 m. Angular sensitivity of magnetisation direction in degrees cannot be exactly related to spatial sensitivity of depth in metres, but nevertheless the shallower curvature of the depth sensitivity curves suggests that depth to the top of magnetisation is less reliably recovered from the inversions than the direction of magnetisation. This is consistent with the difference in depth to the top of the two models of 40 m compared to the difference in their magnetisation directions of ~1°. Horizontal offset of magnetisation is linked to angular error in estimated magnetisation direction but there is no equivalent linkage for vertical offset of magnetisation. It is not feasible to apply significance to the sensitivity curves in Fig. 5.27, but the clear data misfit minima for the magnetisation direction curves provided confidence that these narrow models were sufficiently well qualified to confidently design the drillhole.

5.9 RESOLUTION OF COMPLEXITY OF MAGNETISATION

Voxel inversion models are being created that have both incremental and large stepwise variation in magnetisation direction between immediately adjacent elements. An example is an inversion that reports three joined magnetisations spanning a range of direction of 133° as the source of the Black Hill Norite north-west anomaly (MacLeod and Ellis 2016, their fig. 7). This is the same anomaly investigated in section 5.6 that was already shown to be well explained by a single magnetisation model compatible with nearby rock magnetisation measurements. The three-magnetisation model may well match the anomaly, but its unnecessary complexity cannot be justified and should not be promoted on the grounds that it was generated by a sophisticated computer algorithm. For a well-defined anomaly, a compact single-magnetisation model that successfully matches the anomaly has the only feasible mean magnetisation direction (typically within uncertainties of less than 15°).

Complex distributions of magnetisation can be mapped from magnetic field data if there is at least partial separation between those magnetisations to support their separation. These complex magnetisations are not mapped as reliably as a single magnetisation would be and their analysis and inversion requires greater attention and strategy than for a single magnetisation. Figure 5.28A shows an 11 km diameter complex magnetic field anomaly in the Coompana area of south-west South Australia, measured by the same survey as the anomaly investigated in the previous section. The first issue on inspection of the TMI image is to design a starting model. The anomaly is primarily negative and is due to a mostly reverse but diverse magnetisation. I represent the magnetisation of the central zone of the anomaly (marked ‘a’ in Fig. 5.28B) with a single horizontal sheet of magnetisation with its margin digitised to the step change in the field (and represented by body ‘a’ in the post-inversion model in Fig. 5.29C). There is an outer second step of similar amplitude but mostly sharper gradients that seems to approximately map the extent of a wider body of reverse magnetisation (marked ‘b’ in Figs 5.28B and 5.29C) and I digitised the margin of a second sheet to that magnetic field step. It is not certain from inspection of the TMI anomaly whether the two sheets are vertically or horizontally zoned. In the starting model the two sheets were given similar depths of 500 m and depth extents of 2,000 m, so that inversion

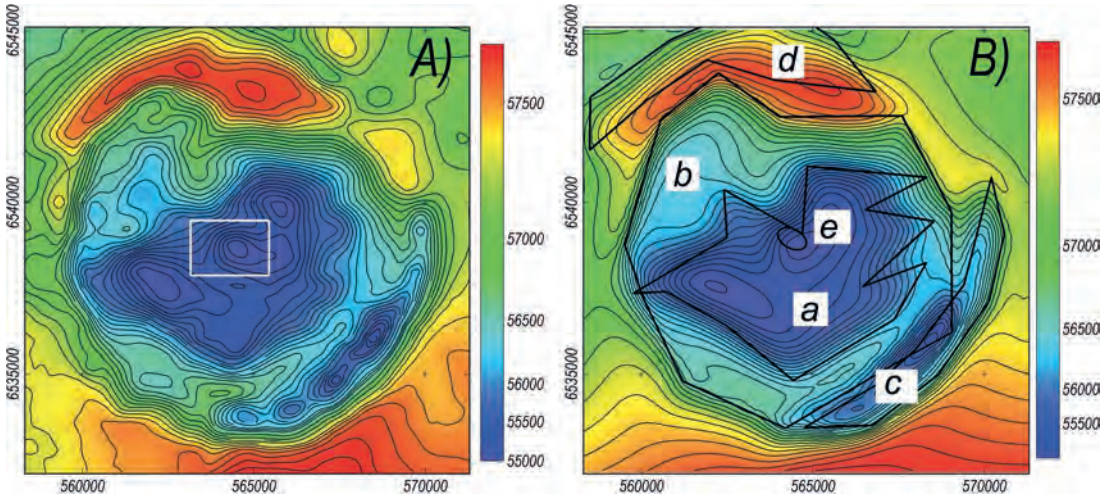

Fig. 5.28. A) TMI anomaly of the south-east complex anomaly in Coompana, south-west South Australia and B) model-computed TMI with outlines of the top extent of the model bodies.

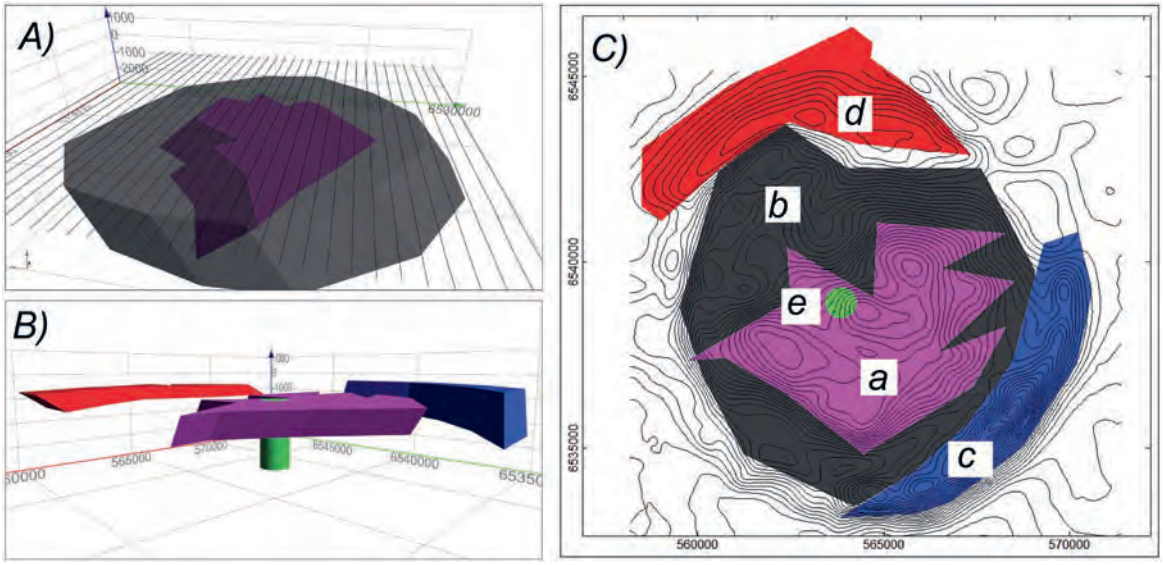

Fig. 5.29. Model components A), B) in perspective view and C) in map view (with TMI contours). Overlap of the inner and outer sheets is shown in A) and in B) the outer sheet is excluded to more clearly show the other components.

could adjust depth to the top and depth extent of each as favoured by the magnetic field data. The major remaining features are a sharp magnetic low to the south-east and a positive to the north, marked 'c' and 'd' respectively in Fig. 5.28B and 5.29C. I then managed the inversion (performed with the ModelVision software) in a series of stages, applying manual forward-modelling adjustments as advantageous to encourage conversion to a meaningful model. I call this process of prior design of a model and its manipulation throughout the inversion process 'user-guided' inversion. Those who trust in full automation of inversion see human intervention as a contamination of the inversion process and an unwanted introduction of human bias. My argument is that inversion of this degree of complexity benefits from guidance of a higher authority, and that inversion code is only a tool to be applied with understanding and skill to generate a geologically acceptable explanation of the measured magnetic field. Documentation of the inversion and decision history (such as provided here) is important for evaluation of the models that are produced.

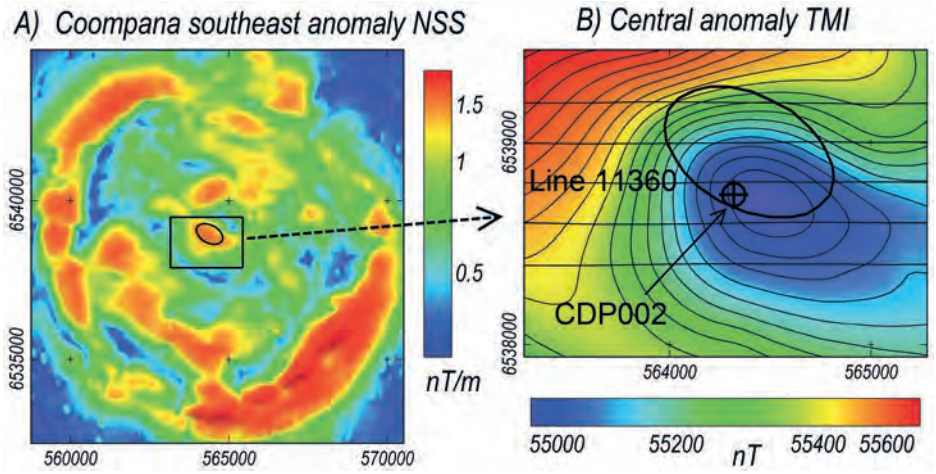

Fig. 5.30. A) NSS of TMI of the south-east complex anomaly in Coompana and B) TMI of the inset box in A with east–west flightlines, outline of the top of the elliptic-section pipe model and location of drillhole CDP002.

I progressed the inversion in a series of steps, starting with addressing the major features and ending with addition of details as justified and required. The first step allowed adjustment of the depth, depth extent, magnetisation strength, magnetisation direction and background field parameters. This produced a surprisingly close match to the measured field, confirming that the basic model concept was feasible. The inversion assigned a greater depth and smaller depth extent to the central sheet than to the outer one, so that the two sheets appear to have similar base depths (although these depths are poorly constrained). The central sheet overlaps the outer sheet in all locations, and in consequence there is no need to introduce additional complexity of a contact between them. Instead the central sheet has the summed magnetisations of both overlapping components. After minor adjustments, in the next step I allowed the bodies to move horizontally and to plunge, and subsequently I allowed the bodies to reshape by adjusting the horizontal coordinates of their vertices. Each step of inversion included multiple iterations. Bounds were set on each parameter to encourage a steady convergence by multiple small steps. In any one iteration, if a reduction in data misfit was achieved the inversion adjusted to search a reduced model space in more detail. If no improvement was achieved the inversion investigated a larger model space to evaluate if it was stalled in a local minimum. After each change all model views in map, cross-section and/or perspective windows are updated, together with all displays of the computed field. In this way I was able to track live progress of the inversion, interrupt it to stop unwanted changes or to plan the next set of changes.

In the last stages of the inversion, the local minima in the centre of the anomaly began to emerge as significant residual data misfits and I introduced an additional vertical circular pipe to represent a possible feeder zone (at location 'e' in Fig. 5.29B and shown as body 'e' in the inversion model in Fig. 5.29C). Even at this late stage of the inversion the influence of this body is so diluted within the complete model that it is not reliably constrained. This local feature is one of several that have distinct expressions in the NSS transform (Fig. 5.30A) and was chosen as the location for a drillhole to test the structure. The model of the complete anomaly, covering an area of more than 100 km^2 has the objective of resolving major geological structure and is not suited to define detail at any specific location. To locate and design the borehole a data clip was extracted (shown by the box in Figs 5.28A and 5.30A) that was inverted separately. The flightline cross-sections through this detailed model are shown in Fig. 5.31. The best horizontal-topped plunging elliptic-section pipe returned by the inversion is very different to the corresponding (poorly constrained) body in the full anomaly inversion (depth 900 m) with a depth of 400 m. From the results of the detailed inversion the drillhole (CDP002, Dutch *et al.* 2017b) was located. This drillhole intersected the top of magnetisation (a gabbro) at 366 m below surface, 9% shallower than predicted by the detailed inversion. This is encouraging as the anomaly is not confidently separated from the complex background field and is poorly suited for depth estimation.

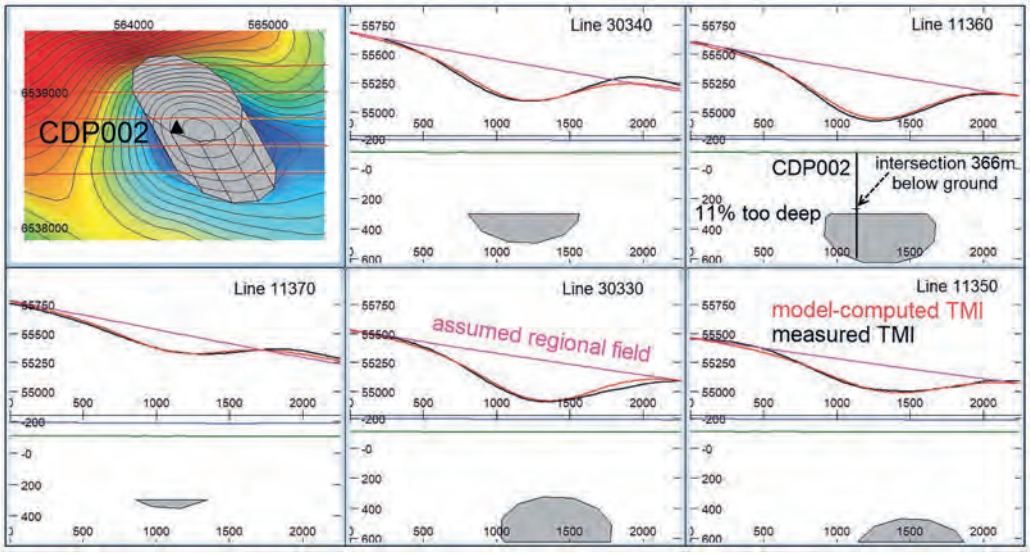

Fig. 5.31. Flightline sections of the central detailed inversion model to design borehole CDP002.

5.10 CONCLUSIONS

The key finding of the main inversion model is to confirm that the magnetic anomaly is consistent with a model that can be geologically interpreted as a (probably differentiated) basic, sub-volcanic intrusive complex, including both sub-horizontal sheets (model bodies 'a' and 'b') and arcuate fracture infillings (bodies 'c' and 'd'). This model can be incorporated into mineral exploration programs, and components of the model such as possible feeder zones and contacts between internal units or with surrounding basement can be targeted in concept-driven models of possible areas of mineralisation. The detailed model of the central section of the anomaly successfully predicted a depth for design of a borehole to test that feature.

For this complex model, inversion should not be considered complete but to have reached a stage at which further development is not warranted until answers to any specific questions are required and a targeted upgrade of the model can be performed. There are still imperfections in terms of unwanted overlap of model components at a few locations and residual data misfits. Magnetisations of the different model components are listed in Table 5.1 (including adjustment of magnetisation values for body overlaps where appropriate).

An argument against inversions such as these and favouring greater automation and less supervision is that automated inversions are performed much more quickly and require less geological understanding of the operator. However, the time required for a user-guided inversion such as this example should not just be compared against the computation time of an automated inversion but in context of the time and expense to plan, contract and acquire the survey, process and

Table 5.1. Volume, top depth (metres below surface) and resultant magnetisation of the model bodies.

Model	Description	Volume (km^3)	Depth to top (m)	Intensity A/m	Declination	Inclination
a	Inner sheet	17.2	750	12.9	30	+45
a*	Corrected for b overlap			16.1	18	+52
b	Outer sheet	79.8	170	3.5	322	+46
c	Negative southern	7.4	360	8.5	15	+40
d	Positive northern	5.0	490	6.0	186	−14
e	Central pipe	0.94	910	26.5	266	+4
e*	Corrected for b overlap			28.3	270	+11
e'	Dedicated local inversion	0.123	405	7.8	33	+51
e'*	Corrected for b overlap			11.2	12	+58

analyse the data, make the necessary interpretation decisions based on the results and make the financial commitments for any drilling. Saving a few days of inversion time at the cost of less informed decisions is a false economy given that even minor details of inversion results might be of critical importance to the project objectives and determine between success and failure.

REFERENCES

Baranov V, Naudy H (1964) Numerical calculation of the formula of reduction to the magnetic pole. *Geophysics* **29**, 67–79. doi:10.1190/1.1439334

Beiki M, Clark DA, Austin JR, Foss CA (2012) Estimating source location using normalized magnetic source strength calculated from magnetic gradient tensor data. *Geophysics* **77**, J23–J37. doi:10.1190/geo2011-0437.1

Blakely RJ (1995) 'Potential Theory in Gravity and Magnetic Applications'. Cambridge University Press. pp. 441.

Clark DA (2014) Methods for determining remanent and total magnetisations of magnetic sources – a review. *Exploration Geophysics* **45**, 271–304. doi:10.1071/EG14013

Dannemiller N, Li Y (2006) A new method for determination of magnetisation direction. *Geophysics* **71**, L69–L73. doi:10.1190/1.2356116

Dutch RA, Jagodzinski EA, Pawley MJ, Wise TW, Tylkowski L, Lockheed A, McAlpine SRB, Heath P (2017a) 'Drillhole CDP007 preliminary field-data report'. PACE Copper Coompana Drilling Project: Report Book 2017/00044. Department of the Premier and Cabinet, South Australia, Adelaide.

Dutch RA, Jagodzinski EA, Wise TW, Pawley MJ, Tylkowski L, Lockheed A, McAlpine SRB, Heath P (2017b) 'Drillhole CDP002 preliminary field-data report'. PACE Copper Coompana Drilling Project: Report Book 2017/00038. Department of the Premier and Cabinet, South Australia, Adelaide.

Foss CA (2006) 'Evaluation of strategies to manage remanent magnetisation effects in magnetic field inversion'. 76th Annual International Meeting. *SEG Expanded Abstracts*, 938–942.

Foss CA, McKenzie KB (2011) Inversion of anomalies due to remanent magnetisation: An example from the Black Hill Norite of South Australia. *Australian Journal of Earth Sciences* **58**, 391–405. doi:10.1080/08120099.2011.581310

Foss CA, Leslie K, Schmidt PW (2021) 'If you can't go to the anomaly then let the anomaly come to you'. Extended abstract, AEGC Brisbane, pp. 1–4.

Helbig K (1963) Some integrals of magnetic anomalies and their relation to the parameters of the disturbing body. *Zeitschrift für Geophysik* **29**, 83–96.

Hood PJ (1964) The Königsberger ratio and the dipping dyke equation. *Geophysical Prospecting* **12**, 440–456. doi:10.1111/j.1365-2478.1964.tb01916.x

Lourenço JS, Morrison HF (1973) Vector magnetic anomalies derived from measurements of a single component of the field. *Geophysics* **38**, 359–368. doi:10.1190/1.1440346

MacLeod I, Ellis R (2016) 'Quantitative Magnetisation Vector Inversion'. ASEG Extended Abstracts 2016, 1–6. doi:10.1071/ASEG2016ab115

Nabighian MN (1972) The analytic signal of two-dimensional magnetic bodies with polygonal cross-section: its properties and use for automated anomaly interpretation. *Geophysics* **37**, 505–517. doi:10.1190/1.1440276

Paine P, Haederle M, Flis M (2001) Using transformed TMI data to invert for remanently magnetised bodies. *Exploration Geophysics* **32**, 238–242. doi:10.1071/EG01238

Phillips JD (2005) Can we estimate total magnetisation directions from aeromagnetic data using Helbig's integrals?. *Earth, Planets, and Space* **57**, 681–689. doi:10.1186/BF03351848

Rajagopalan S, Schmidt PW, Clark DA (1993) Rock magnetism and geophysical interpretation of the Black Hill Norite, South Australia. *Exploration Geophysics* **24**, 209–212. doi:10.1071/EG993209

Schmidt PW, Clark DA (1997) Directions of magnetisation and vector anomalies derived from total field surveys. *Preview* **70**, 30–32.

Schmidt PW, Clark DA (1998) The calculation of magnetic components and moments from TMI: a case study from the Tuckers igneous complex, Queensland. *Exploration Geophysics* **29**, 609–614. doi:10.1071/EG998609

Schmidt PW, Clark DA, Rajagopalan S (1993) An historical perspective of the Early Palaeozoic APWP of Gondwana: new results from the Early Ordovician Black Hill Norite of South Australia. *Exploration Geophysics* **24**, 257–262. doi:10.1071/EG993257

Zietz I, Andreasen GE (1967) Remanent magnetisation and aeromagnetic interpretation. *Mining Geophysics* **2**, 569–590.